

# Comparison of Two Folded Methods of Solar Sails

Laohu Yuan<sup>1</sup>, Rui Song<sup>1</sup>, Feng Wang<sup>2</sup>, Jianzheng Wei<sup>3</sup> and Jiafu Liu<sup>4,\*</sup><sup>1</sup> College of Aerospace Engineering, Shenyang Aerospace University, Shenyang 110136, China<sup>2</sup> Liaoning General Aviation Academy, Shenyang 110136, China<sup>3</sup> School of Astronautics, Harbin Institute of Technology, Harbin 150001, China<sup>4</sup> School of Aeronautics and Astronautics, Sun Yat-sen University, Shenzhen 518107, China

\* Correspondence: liujf53@mail.sysu.edu.cn

**Abstract:** The solar sails can be deployed by jointed truss or by inflated support tube. The deployed process and final deployed state of the solar sails is closely related to the design of the deployed mechanism. Therefore, the design of the deployed mechanism is very important for this new type of spacecraft. In this paper, we study the problem of the inflatable deployment of the solar sail; we utilized MSC.Patran to build the Z-folded and the Z+ curly-folded finite element models. LS-DYNA was used to simulate the dynamic characteristics of the above two solar sails under different conditions, and the results were analyzed. The results show that in the model that adopted the Z-folded method, the deployed process is relatively stable, and the effect of deployment is good, which is more suitable for practical application.

**Keywords:** solar sails; deploy; folded support tubes; finite element; dynamic characteristics

## 1. Introduction

The solar sail is a new type of spacecraft with novel concepts and broad prospects. To achieve continuous propulsion, the spacecraft relies on the ultra-thin sail surface, which is heavy yet incredibly light. By far, it is the only spacecraft that does not require a considerable amount of chemical fuel and working medium for flight control; hence, its life in orbit is not restricted by fuel, and the high-performance materials can make the solar sails lighter, enormously reducing the mass of the launch and further saving the cost of the mission.

The deploying dynamics of a solar sail is one of the critical technologies to complete its orbit mission. Mechanical and inflatable solar sail deployment technologies are the most common. The mechanical deployment utilizes a truss with joints as the mechanism. There are many alternative methods for inflating the solar sail. At present, the most widely used method is the volume control method. Glaser R. et al., 2004 used three inflatable methods to deploy a quasi-static thin membrane space structure, namely CV, CP, and ALE methods, and conducted analysis furthermore experiments [1].

Different deployed mechanisms can be designed based on a variety of theories. Wei J. et al., 2018 proposed a design of a deployable membrane sail with four self-supporting inflated booms, and the folded and deployed scheme of this sail [2], a method for calculating the dynamic characteristics of the inflatable boom considering the influence of inflated pressure, is also given. In addition, the dynamics analysis and on-orbit experiments of the inflatable gravity gradient boom were also completed [3]. Y. Hui et al., 2017 set up dynamic experiment to design and construct the dynamic behaviors. A Phantom V12.1 high-speed camera was applied to record the deployment of the tape-spring hinge [4]. Fernandez J.M. et al., 2011 proposed we can use the bistable winding composites as the deployable boom of solar sails [5]. This structure is easy to expand and may become an ultra-light design. Brown, M.A., 2011 studied a new deployable mast that could provide a way to scale up solar sails to very large sizes, and this new design was compared to the



**Citation:** Yuan, L.; Song, R.; Wang, F.; Wei, J.; Liu, J. Comparison of Two Folded Methods of Solar Sails. *Aerospace* **2022**, *9*, 746. <https://doi.org/10.3390/aerospace9120746>

Academic Editor: George Z. H. Zhu

Received: 6 September 2022

Accepted: 8 November 2022

Published: 23 November 2022

**Publisher's Note:** MDPI stays neutral with regard to jurisdictional claims in published maps and institutional affiliations.



**Copyright:** © 2022 by the authors. Licensee MDPI, Basel, Switzerland. This article is an open access article distributed under the terms and conditions of the Creative Commons Attribution (CC BY) license (<https://creativecommons.org/licenses/by/4.0/>).

latest truss used in NASA solar sails [6]. Qin Dong, 2017 designed a solar sail deployment mechanism with a simple structure, small mass, large contraction expansion ratio and high stability, as well as carried out finite element analysis and optimization [7]. Siyuan Rong et al. utilized MSC.Patran to build the finite element model of the solar sail. The proposed segmented inflatable mode and integral inflatable mode imposed normal restraint control force upon these two ways and simulated deploying dynamics characteristic of the Z-folded solar sail inflatable support tube of the two modes above by LS-DYNA codes [8]. Costanza G. et al., 2016 designed and manufactured a self-deploying system based on NiTi shape memory wires in a small prototype that studied three different types of folded solar sails and used two different nickel–chromium wires as active materials to achieve self-deployment of the sails [9]. T. Sproewitz et al., 2019 provided an overview of the Gossamer-1 hardware development and qualification campaign. The design is based on a crossed boom configuration with triangular sail segments. Using engineering models, all aspects of the deployment were tested under an ambient environment. Several components have also undergone environmental qualification tests [10]. R. Roy et al., 2018 proposed a sail, shaped like a cone, which redirects the incident solar radiation force to appropriately tension itself against deformation. By computing the performance parameters for a hypothetical nano-satellite mission and comparing it to existing mission designs, the advantages of the new design are emphasized [11]. Johnson L. et al., 2011 were the first to demonstrate the deployment of solar sails in orbit. Although they failed, they tremendously promoted the research process of solar sails [12]. Fu B. et al., 2016 reviewed the current state of solar sail technology. People mainly focus on areas such as solar sail dynamics, attitude control, design and deployment, and trajectory analysis [13]. The model of solar radiation pressure and attitude dynamics receives special consideration. Some basics of solar sail that would be extremely useful for a new investigator in the field are also presented [14]. Fernandez J.M., et al. presented a summary of the design and development of a gossamer sail deorbiting system for objects in LEO to assist in the future development of similar concepts. The objective was to give an overall picture of the usefulness and needs of these gossamer structures, show some of the different analyses carried out to established mission requirements, and present the system design, characterization of structural components, and qualification testing process to comply with these requirements [15].

Because the inflatable structure has the advantage of a short construction period and strong resistance to earthquakes, it can be applied to sealed tunnels. Sosa E.M. et al., 2016 proposed inflatable deployment of finite element models to simulate the preliminary deployment and inflation of a large inflatable structure that is used to seal a tunnel and carried out the experiments of the initial deployment of inflatable structures for sealing of rail tunnels [16,17]. Pecora L. et al., 2019 simulated the controlled deflation, folding, deployment, and inflating process of a large-scale inflatable structure with a sealed tunnel cross-section [18]. M. Lou et al., 2000 presented experimental and analytical study results on different types of space inflatable booms, including the self-rigid cable carpenter-tape-reinforced aluminum laminate booms [19]. Mallikarachchi H.M.Y.C. et al. extended the early research of a quasi-static-folded model and deployment to dynamic deployment and simulated and verified the dynamic deployment of spring hinges made of two layers of plain weave carbon fiber laminates through software and experiments [20]. Block J. et al., 2011 proposed two ways to deploy with ultra-light movable arms: one is driven by an inflatable bladder inside a spiral boom, and the other is driven by an electric deployer with a directly driven boom end [21]. Li Q. et al., 2016 performed a series of deployment tests on four small-scale, single-fabric arches and a fully-scale fabric arch frame to study the feasibility of deployment dynamics and deployment. Finite element simulation based on the control volume method was performed to study the self-deployment failure of the arch frame and reveal the development of membrane stress [22].

With the development of technology, to simulate the inflatable process better, the selected materials and structural shapes are changing. Ma Ruiqiang et al., 2018 based on the Timoshenko beam theory and the Hamilton principle, derived the differential

equation of self-supporting arm vibration and proposed a beam element model considering the pre-stress of the inflatable pressure and changes of configuration [23]. Zykov A.V. et al., 2015 used numerical methods to solve the dynamics deployment of weightless tether [24]. For evaluation problems of kinematic accuracy reliability for folding and deploying mechanisms under the condition of a small sample, the continuous contact effective coupling model considering gaps of the kinematic pair was built by using the “effective length model” theory: based on the proposed kinematics model of folding and deploying mechanisms, a simulated method of mechanism kinematic accuracy reliability was proposed by the Monte-Carlo method, and kinematic accuracy reliability for folding and deploying the mechanism of a certain type of missile wing was calculated [25]. Zhang X. et al., 2017 established a simplified model considering the out-of-plane motion of solar sails to qualitatively analyze the dynamics of solar sails when it is rotating. The effects of structural parameters, initial conditions, and feedback control parameters were analyzed to stabilize the process of deployment [26]. Rui W. et al., 2018 designed a reflector of the substructure of a solar sail, which can control the direction and magnitude of solar radiation pressure without changing its direction to the sun [27]. Yang C. et al., 2019 aimed to propose static and dynamic evaluations for a 160 m solar sail by comparing the results obtained from an 8 m deployable prototype. Based on the updating model and parameter modification theory, the finite element analysis (FEA) model of the 8 m prototype was constructed, and results were obtained to validate the effectiveness of the proposed numerical simulation method [28]. Jiafu Liu et al., 2019 studied the dynamics of the highly flexible solar sail subjected to various forces, and the Euler beam model was adopted to represent the whole structure [29]. Jiafu Liu et al., 2018 also considered that we can utilize solar radiation pressure (SRP) to actively control the surface shape of a reflector consisting of a rigid hoop and slack membrane with embedded reflectivity control devices (RCDs). The full non-linear static partial differential governing equations for a reflector with negligible elastic deformations are established for the circumferential, radial, and transverse directions separately [30].

This article first introduces the control volume method and its theoretical model, which is used to describe the interaction between the gas and the airbag. Then, the airbag model and the other keywords are selected. The solar sail adopting the Z-folded and Z+ folded modes carried out a simulation of inflatable deployment to provide accurate predictions.

## 2. Materials and Methods

First, we chose a method that could better describe the interaction between the gas and the airbag, then we chose a suitable airbag model to simulate the inflatable model, and finally we chose the corresponding contact keyword to reflect the interaction.

### 2.1. Summary of Control Volume Method

The control volume method can take the load curve as the gas filling condition to simulate the interaction with the membrane structure. To some extent, this method ignores the gas inertia problem that needs to be considered in the inflation process but also takes into account the pressure generated by the gas. Its basic principle is to disperse the internal control volume of the membrane structure into multiple connected cavities with assumed diaphragms. This method presumes that the pressure in the cavity is equal at each time, and the gas flowing from one cavity to the next is a function of the diaphragm area. When the inflation starts, the proportion of the diaphragm section increases continuously; when the membrane structure is completed and unfolded, the extent of the diaphragm section will not expand and should be equal to its sectional area. Therefore, this method can well approximate the state of the gases inside the continuously expanding inflatable structure, and the calculation pressure is less.

Radek Glaser et al. [1] conducted a comparative inflation study that presents a cross-comparative summary of the three (CV, CP, ALE) inflation approaches that utilize an explicit finite element and experimental inflation methodologies applied to large, thin, and

light semi-spherical/cylindrical/semi-spherical deployable space structures. According to their study, the CV method is preferred for problems involving large and simple shape inflatables with a quasi-static response where the computational time is of the essence and the high accuracy of the gas behavior is not required.

In this paper, for practical engineering concerns, the CV method should be used to estimate the deployment dynamic characteristics of the solar sail.

When selecting the CV method to study the inflatable structure, the inflatable structure is used as a control volume, the surface of the inflatable structure is the control surface of the body, and the cavity inside the inflatable structure is the control volume. The model is shown in Figure 1.

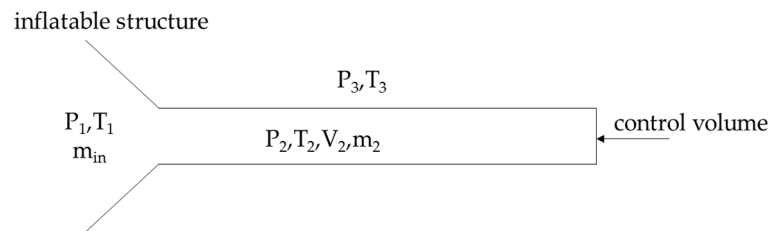


Figure 1. Model of inflatable structure.

Where the formula of volume is:

$$V = \iiint_{\Omega} dv \tag{1}$$

where  $\Omega$  represents the enclosed space formed by the inflatable structure. According to Green’s formula, the volume integral enclosed by the area of the closed surface can be calculated as follows:

$$V = \iiint_{\Omega} dv = \oiint_{\Gamma} xndS = \sum_{i=1}^N \iint_{\Gamma_i} xndS = \sum_{i=1}^N \bar{x}_i n_i S_i \tag{2}$$

where  $x_i$  represents the average of the  $i$ -th unit in the  $x$  axis,  $n_i$  represents the direction cosine of the unit normal vector, and  $S_i$  represents the area of the  $i$ -th unit.

LS-DYNA uses the central difference to integrate time, and the acceleration of each node of the mechanism at the end of the  $n$ -th time step is calculated by the following formula:

$$\{\ddot{D}\}_{t_n} = [M]^{-1} \left[ \{R^{ext}\}_{t_n} - \{F^{int}\}_{t_n} \right] \tag{3}$$

where  $\{\ddot{D}\}_{t_n}$  is the acceleration of the structure at the end of the  $n$ -th time step,  $[M]$  is the mass matrix,  $\{R^{ext}\}$  is the nodal external force applied on the structure at the end of the  $n$ -th time step (including the equivalent nodal force transformed by the distributed load), and  $\{F^{int}\}$  is the internal force vector of the structure at time  $t_n$ , generally composed of the following items:

$$F^{int} = \int_W B^T sdW + F^{hg} + F^{contact} \tag{4}$$

$\int_W B^T sdW$  represents the equivalent nodal stress of the element stress field at time  $t_n$ .  $F^{hg}$  is the hourglass resistance, and  $F^{contact}$  is the contact force.

According to the basic idea of the central difference, acceleration is the first-order central difference of velocity, and velocity is the first-order central difference of displacement. Therefore, the following Formulas (5)–(9) can be used for analysis and calculation of them:

$$\left[ \left\{ \dot{D} \right\}_{t_{n+\frac{1}{2}}} - \left\{ \dot{D} \right\}_{t_{n-\frac{1}{2}}} \right] / \left[ \frac{1}{2} \Delta t_{n-1} + \Delta t_n \right] = \left\{ \ddot{D} \right\}_{t_n} \tag{5}$$

$$\left[ \left\{ U \right\}_{t_{n+1}} - \left\{ U \right\}_{t_n} \right] / \Delta t_n = \left\{ \dot{D} \right\}_{t_{n+\frac{1}{2}}} \tag{6}$$

where

$$\begin{aligned} \Delta t_{n-1} &= t_n - t_{n-1}, \Delta t_n = t_{n+1} - t_n \\ \Delta t_{n-\frac{1}{2}} &= \frac{1}{2}(t_{n-1} + t_n), \Delta t_{n+\frac{1}{2}} = \frac{1}{2}(t_{n+1} + t_n) \end{aligned} \tag{7}$$

The displacement at time  $t + \Delta t$  is as follows:

$$\left\{ D \right\}_{t+\Delta t} = \left\{ D \right\}_t + \left\{ U \right\}_{t+\Delta t} \tag{8}$$

$\left\{ D \right\}_{t+\Delta t}$  is the displacement of the structure at time  $t + \Delta t$ ,  $\left\{ D \right\}_t$  is the displacement of the structure at time  $t$ , and  $\left\{ U \right\}_{t+\Delta t}$  is the increment of displacement.

The expression of the differential form of (6) is as follows:

$$\left[ \frac{1}{\Delta t^2} [M] + \frac{1}{2\Delta t} [C] \right] \left\{ D \right\}_t = \left\{ R^{ext} \right\}_{t-\Delta t} - [K] \left\{ D \right\}_{t-\Delta t} + \frac{1}{\Delta t^2} [M] (2 \left\{ D \right\}_{t-\Delta t} - \left\{ D \right\}_{t-2\Delta t}) + \frac{1}{2\Delta t} [C] \left\{ D \right\}_{t-2\Delta t} \tag{9}$$

where  $\Delta t$  is the time step for calculation, which can be used to compute  $\left\{ D \right\}_t$  and obtain the shape of structure at time  $t$ . When the damping matrix and mass matrix are simplified to diagonal matrix by adopting the block program, this method can greatly improve the efficiency of the solution.

### 2.2. Airbag Model

Select the keyword \*AIRBAG\_SIMPLE\_AIRBAG\_MODEL as the airbag model, which is inflated smoothly. Use the keyword \*MAT-FABRIC as the air bag material. The main power for deploying the inflatable membrane structure is the self-contact of it. Select the keyword \*CONTANCT\_AIRBAG\_SINGLE\_SURFACE. This method will perform two-way retrieval when checking the penetration so that it can effectively prevent the penetration. In the deployed process of the structure, in order to make the model converge, the full integration algorithm is adopted, so there is no need to set the hourglass control.

The Figure 2 shows the theoretical model of the inflatable structure, which is separated into a series of cavities by the diaphragm. The cavity is composed of the outer wall of the structure and the diaphragm. The amount of gas flowing from one cavity to the next cavity is a function of the diaphragm area. As the diaphragm area increases, the inflatable structure deploys. Finally, the inflatable structure is fully deployed, and the opening area is equal to the cross-sectional area of it.

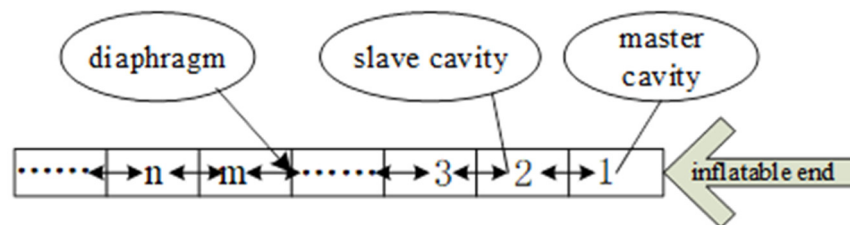
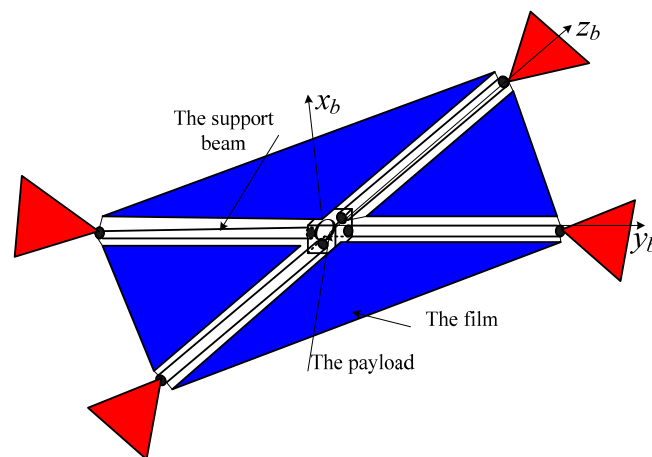


Figure 2. Inflatable model of the support tube.

### 3. The Finite Element Model and Deployed Dynamic Analysis of the Solar Sail

As shown in the Figure 3, in order to explain the problem and simplify it, we first establish a finite element model of a square solar sail with a side length of about 8 m. The length of each support tube is about 5.6 m, and the support tube is connected with the sail surface by infinite points.



**Figure 3.** Schematic diagram of solar sail.

The defaulting unit system when modeling is kg-mm-s-K. The material and geometric dimensions of the inflatable tubes and sail surface are shown in Table 1 below.

**Table 1.** Material parameters and geometric dimensions of inflatable tube and sail surface.

Composition	$\rho$ (kg/mm <sup>3</sup> )	E (GPa)	Poisson's Ratio $\nu$	Thickness (mm)
Support tube	$1.42 \times 10^{-6}$	2.5	0.34	0.1
Sail surface	$1.42 \times 10^{-6}$	2.5	0.34	0.0025

### 3.1. Dynamics Simulation of Z-Folded Solar Sail

The finite element model of the solar sail adopting the Z-folded method is established in MSC.Patran as shown Figure 4:

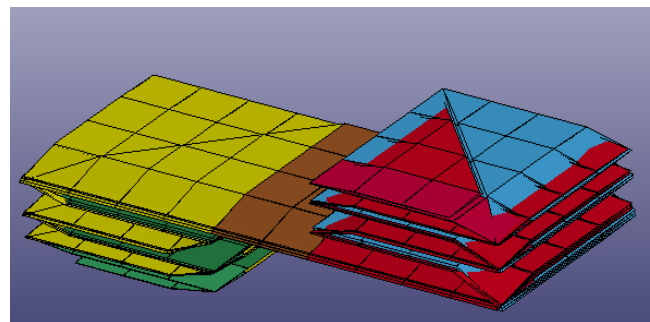


**Figure 4.** Z-folded finite element of solar sail.

Firstly, set one of the conditions as the standard inflation parameter. On this basis, the kinetics results of inflatable deployment under different parameters are obtained by modifying the inflatable rate, the inflatable temperature, and the inflatable pressure. It can be noticed in Table 2.

**Table 2.** Various conditions of the Z-Folded Solar Sail.

Condition Name	Condition Label
standard	1
modify the inflatable rate	2
change the inflatable temperature	3
change the inflatable pressure	4

In condition 1, the dynamic results of inflatable deployment are as follows in Figures 5–8:

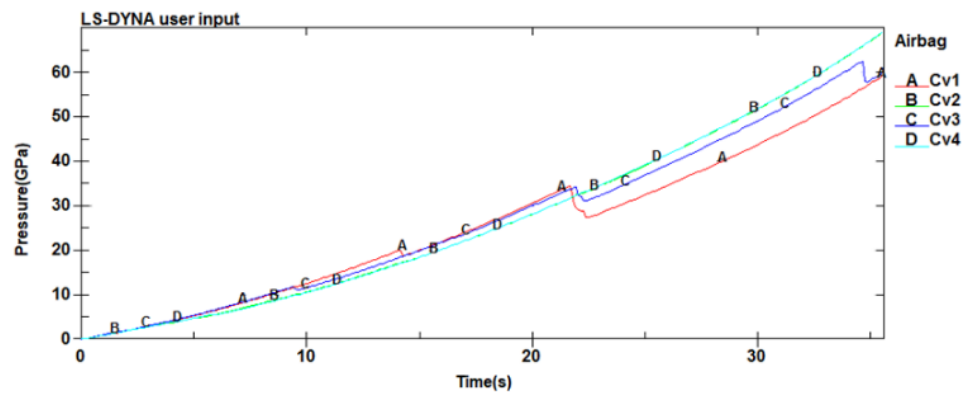


Figure 5. Pressure function curve of each tube under Z-folded and condition 1.

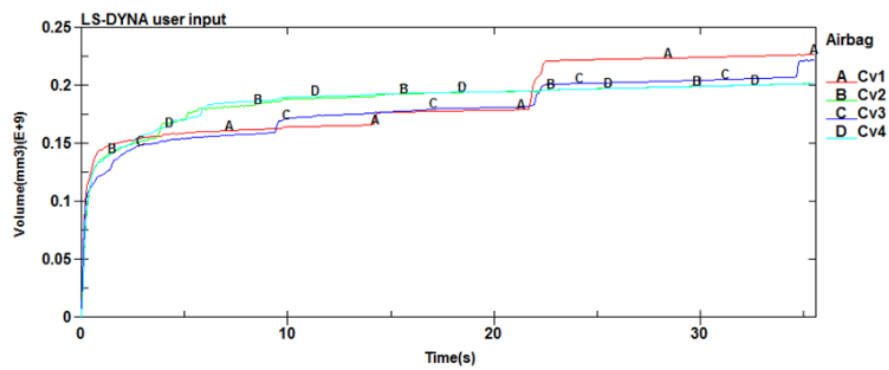


Figure 6. Volume function curve of each tube under Z-folded and condition 1.

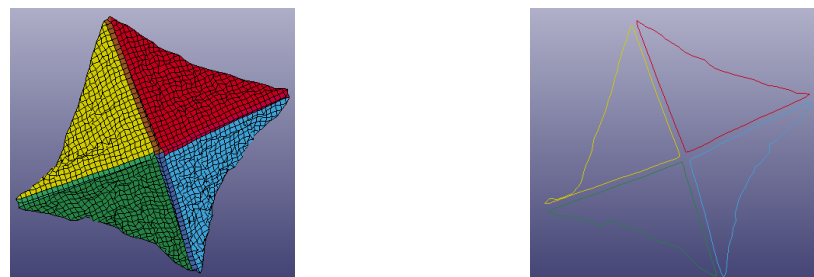


Figure 7. View of fully deployed under Z-folded and condition 1.

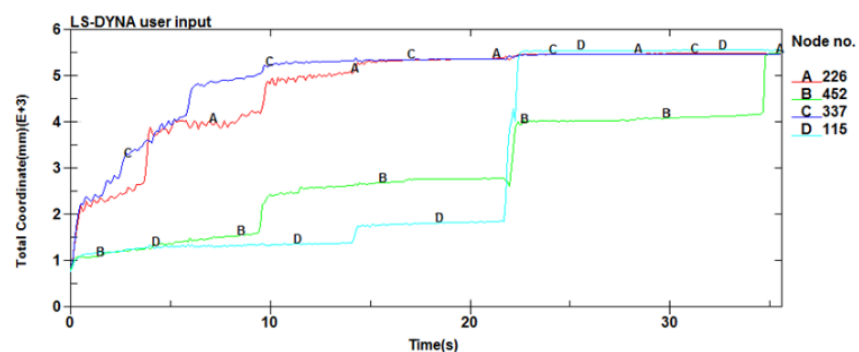


Figure 8. Position of the end nodes of the support tube under Z-folded and condition 1.

The four inflation tubes inflate at the same time. The AC tube expands against the BD tube, which is a pair of inflation tubes located at the outermost side of the folding structure. The BD tube has been unfolded steadily, while the volume of the AC tube is smaller than that of the BD tube at the initial stage, but after the BD tube is fully unfolded, the volume of the AC tube is slightly larger than that of the BD tube. The pressure change curve of the inflation tube is inversely proportional to the volume change curve of the inflation tube. Regarding the results of the volume change curve of the inflation tube, we can see that, in the initial inflation deployment stage, since the volume of the BD tube is greater than the volume of the AC tube, the gas pressure in the BD tube is less than the gas pressure in the AC tube. In the final stage of inflation and deployment, if the volume of the BD tube is smaller than that of the AC tube, the gas pressure in BD tube is greater than that in the AC tube, which is consistent with the results in Figure 5. It also can be seen from Figures 5 and 6 that the pressure and the volume of the tube are stable during the deployment. It can be seen from Figure 8 that there is a relatively strong movement of the tube between 21 s and 25 s and between 34 s and 36 s. The reason is that the elastic modulus of the support tube is large, and the inflatable torque cannot overcome the elastic potential energy during the deployment. Only a certain amount of inflatable torque can be accumulated slowly to force the support tube to deploy. In general, the solar sail support tubes deployed completely in the axial direction in this condition, and the deployed effect is good.

In condition 2, the dynamic results of inflatable deployment are as follows in Figures 9–12:

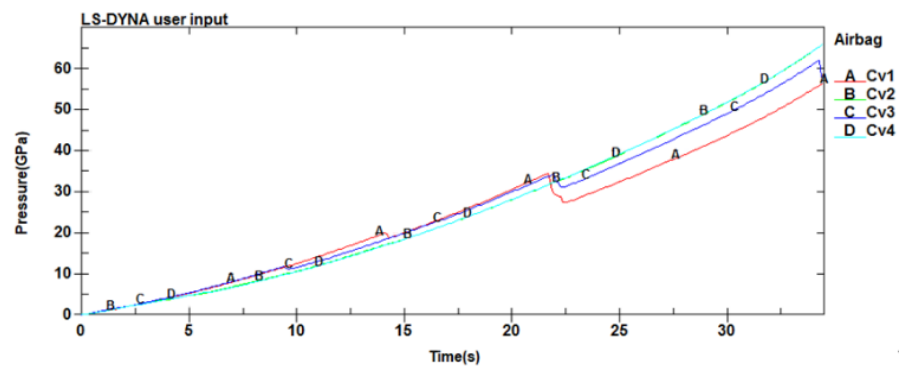


Figure 9. Pressure function curve of each tube under Z-folded and condition 2.

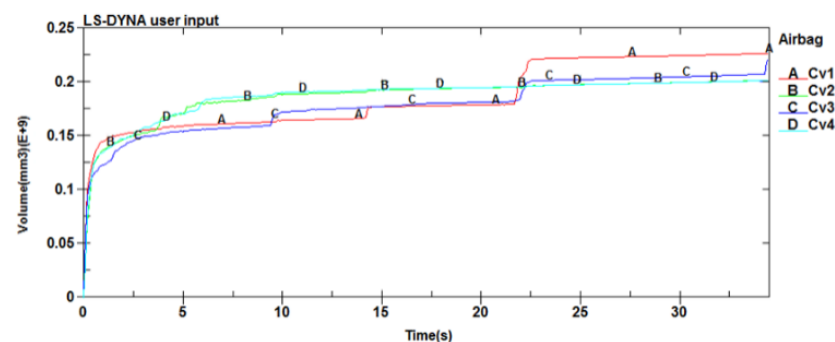


Figure 10. Volume function curve of each tube under Z-folded and condition 2.



Figure 11. View of fully deployed under Z-folded and condition 2.

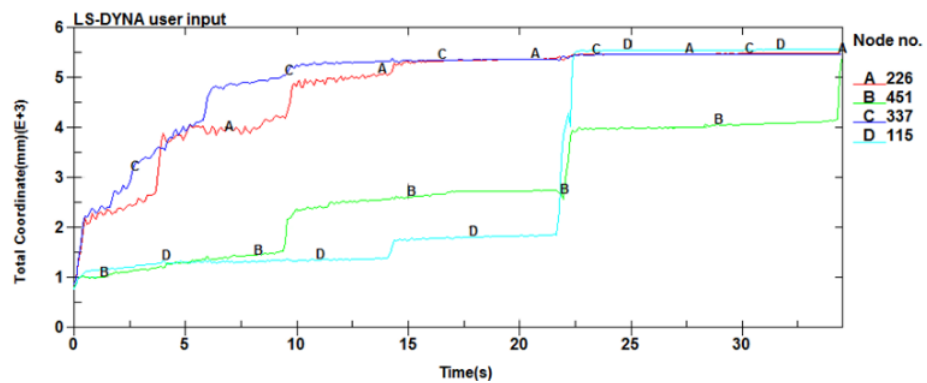


Figure 12. Position of the end nodes of the support tube under Z-folded and condition 2.

Between 3 and 24 s, the volume of the BD tube is always larger than that of the AC tube, because the volume of the BD tube is bound to be larger when it is pushed by the AC tube. Once the AC tube is unfolded, its volume will be slightly larger than that of the BD tube, but generally speaking, its volume difference is not very large. It can be seen from Figure 10 that the volume of the four tubes after being fully deployed is not large. It can be seen from Figure 12 that the end positions of the four support tubes have approximately reached 5.6 m, so the deployed effect is good. However, the node D and the node B suddenly deployed at around 24 and 34 s, respectively, which is not conducive to the deployment of the solar sail. This situation should be avoided as much as possible to achieve a smooth process. It can be seen from Figure 11 that the deployed size of the solar sail meet the requirements.

In condition 3, the dynamic results of inflatable deployment are as follows in Figures 13–16:

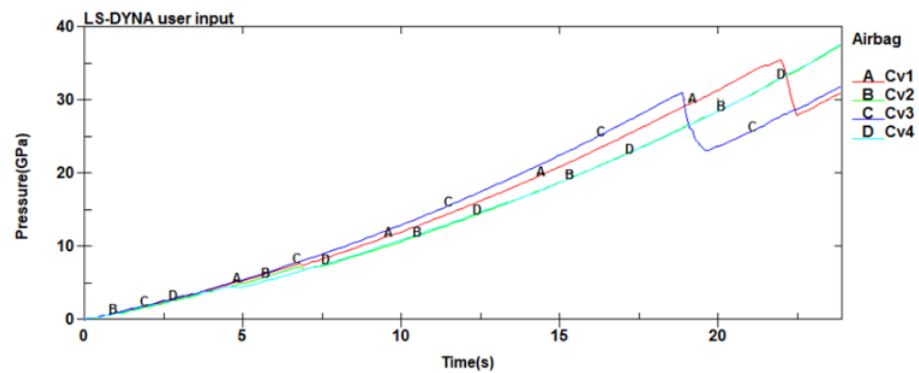


Figure 13. Pressure function curve of each tube under Z-folded and condition 3.

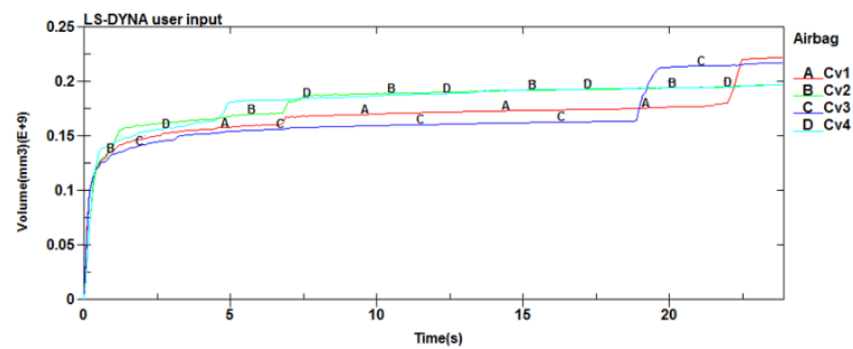


Figure 14. Volume function curve of each tube under Z-folded and condition 3.

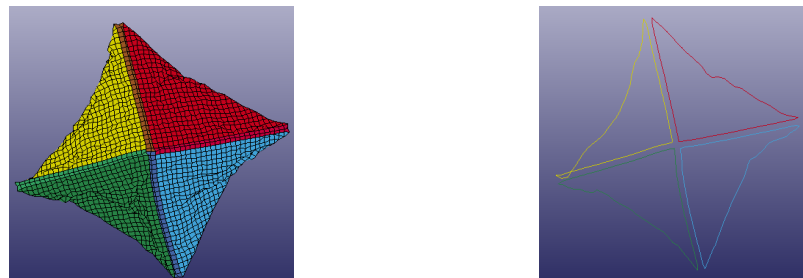


Figure 15. View of fully deployed under Z-folded and condition 3.

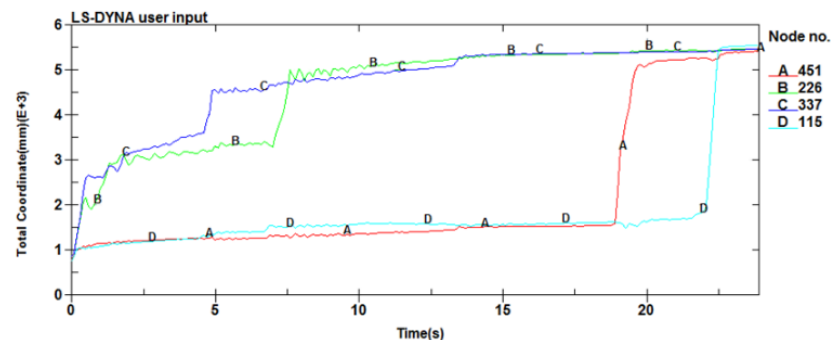


Figure 16. Position of the end nodes of the support tube under Z-folded and condition 3.

It can be seen from Figure 13 that the gas pressure in the inflation tube inside the folding structure increases before the gas pressure in the inflation tube outside the folding structure. In the initial inflation phase, referring to the volume change curve of the inflation tube, the gas pressure in the four inflation tubes is the same. After 4 s, the gas pressure in the four inflation tubes is slightly different, but not very large. At 18 s, the gas pressure in the AC pipe suddenly changes greatly, which indicates that the membrane structure will have pressure hysteresis during the deployment process. That is, when the gas fill passes through the diaphragm, the diaphragm will have an obstruction effect. With the inflation process, the sectional area of the diaphragm will gradually increase. At this time, part of the gas will flow into the next control volume chamber, and the pressure in the pipe will decrease. When the inflation process continues, the pressure will continue to increase, which also corresponds to the volume change curve. The volume keeps increasing, and the gas in the inflation tube keeps flowing forward. When encountering the barrier of the diaphragm, the pressure will increase slightly based on the previous moment. It can be seen from Figure 14 that when the membrane tube is inflated at the set gas temperature, the volume difference of the four inflation tubes in the initial inflation phase is small. However, after 4 s, the volume difference of the four inflation tubes was revealed. The deployment of the BD tube has been relatively stable, and it was always larger than the volume of the AC tube 18 s ago. After the BD tube was fully deployed, the volume of the AC tube

suddenly increased to the maximum, accompanied by severe movement. At this time, the volume of the AC tube is slightly larger than the volume of the BD tube. It can be seen from Figure 15 that the solar sail support tubes deployed well, and though the red edge is slightly loose, the overall deployed state is good. It can be seen from Figure 16 that the support tubes approximately reached about 5.6 m after they had deployed, which achieves the expected effect.

In condition 4, the dynamic results of inflatable deployment are as follows in Figures 17–20:

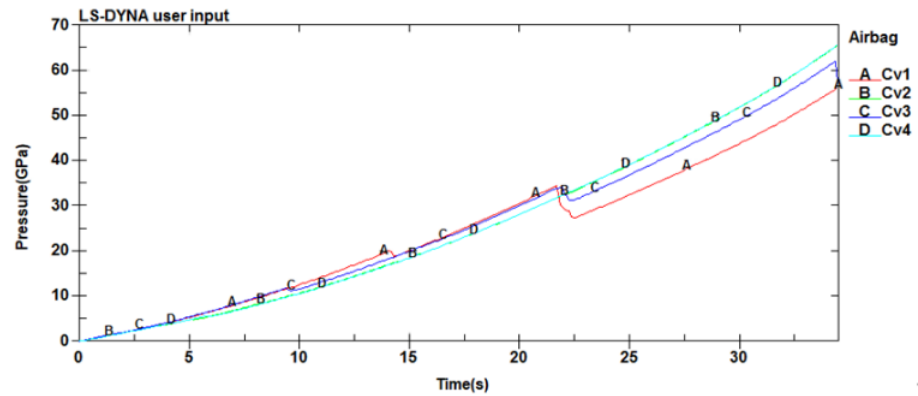


Figure 17. Pressure function curve of each tube under Z-folded and condition 4.

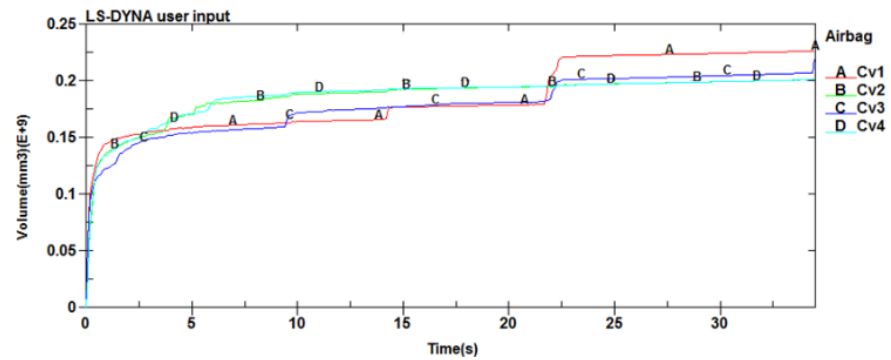


Figure 18. Volume function curve of each tube under Z-folded and condition 4.



Figure 19. View of fully deployed.

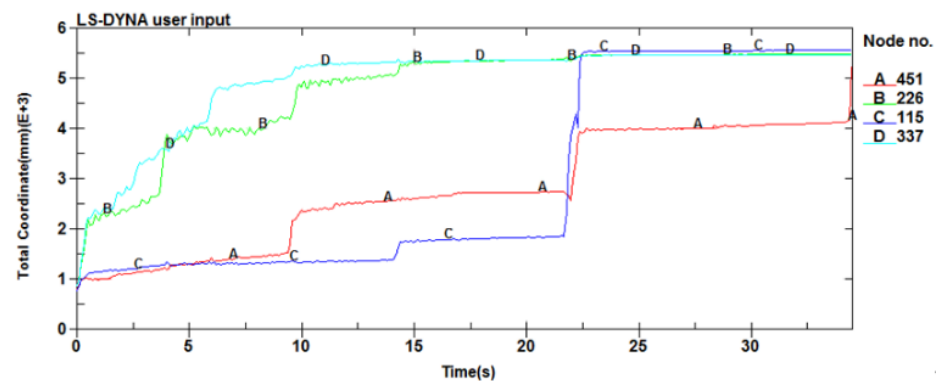


Figure 20. Position of the end nodes of the support tube under Z-folded and condition 4.

It can be seen from Figure 18 that the volume of the BD tube increases preferentially. This is because the BD tube is located at the outer side of the folding structure, and the inner inflation tube is applied with pressure by the outer side. Therefore, the volume of the inflation tube at the outer side of the folding structure increases preferentially over that at the inner side. The volume of each tube increases with time, and the volume of the membrane tube tends to be consistent after being fully expanded. In addition, the volume of each tube fluctuates due to the influence of the dynamic expansion of the structure. It can be seen from Figure 20 that the displacement curves of nodes A and C have a large, sudden change in about 22 s. This is because the membrane element without bending stiffness cannot resist the resilient elastic deformation, which affects the stability of the structure during inflation and deployment. However, the length of the four supporting pipes reached 5.6 m, and the expansion size met the requirements. In addition, in Figure 20, Node B and Node D move back and forth during the initial inflation phase, and about 5 s after inflation, that is, the curve fluctuates slightly. This is because the continuously filled gas accumulates a certain amount of kinetic energy in the membrane tube, which is converted into the elastic potential energy of the structure. The inflation tube of the membrane unit without bending stiffness cannot resist the resilient elastic strain. In condition 4, the inflated pressure is changed by adjusting the inflated load. It can be seen from Figure 18 that the deploying process of the support tubes is relatively stable without much fluctuation. How optimize the inflated load and making the support tubes deploy smoothly is an important concept, which is conducive to the deployment of solar sails in orbit, and sudden deployment is harmful to practical operation.

### 3.2. Dynamics Simulation of Z+ Curly Folded Solar Sail

The finite element model of the solar sail adopting the Z-folded method is established in MSC.Patran as shown below in Figure 21:

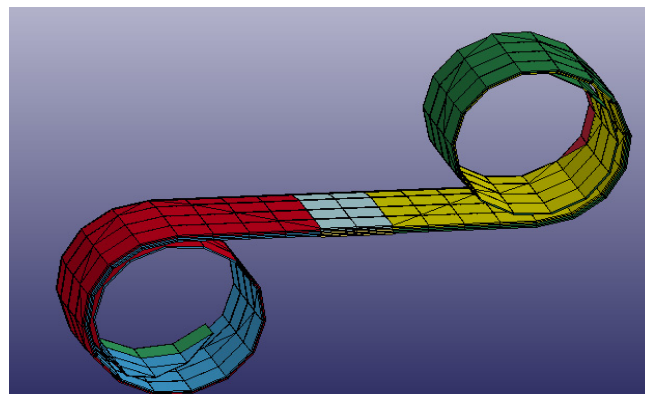


Figure 21. Z+ Curly-Folded finite element of solar sail.

For the Z-folded model, dynamics simulation is performed according to the following five conditions: First, set a standard inflation parameter, and then only the inflatable position, inflatable rate, inflatable temperature, and inflatable pressure are modified to study the effects on deployment. It can be noticed in Table 3.

**Table 3.** Various conditions of the Z+ Curly Folded Solar Sail.

Condition Name	Condition Label
standard	1
modify the inflatable rate	2
change the inflatable position	3
change the inflatable pressure	4
change the inflatable temperature	5

In condition 1, the dynamic results of inflatable deployment are as follows in Figures 22–25:

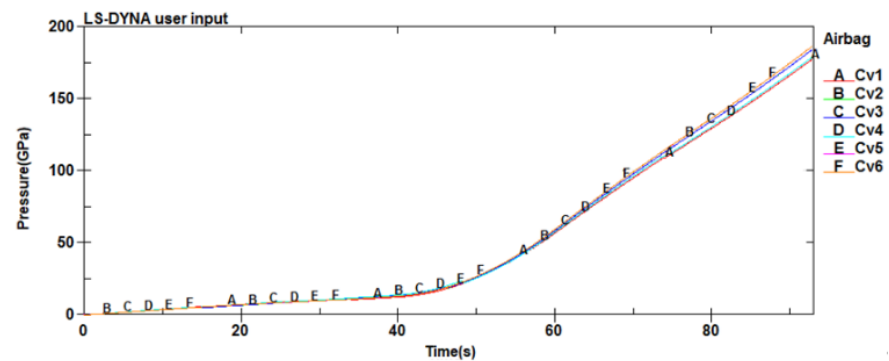


**Figure 22.** Pressure function curve of each tube under Z+ Curly folded and condition 1.

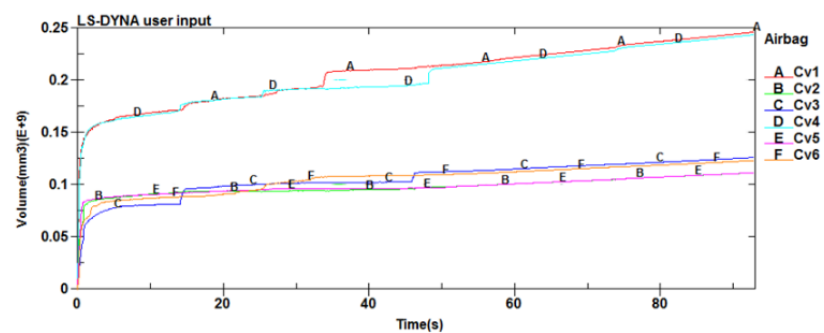


**Figure 23.** Volume function curve of each tube under Z+ Curly folded and condition 1.

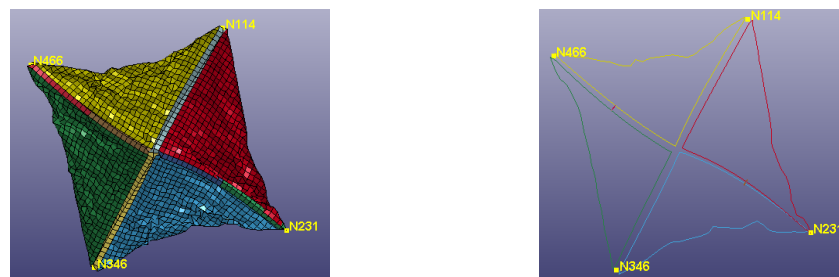


**Figure 24.** View of fully deployed under Z+ Curly folded and condition 1.

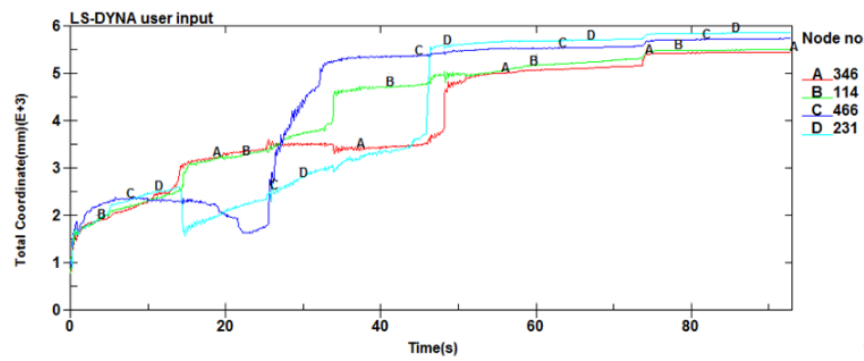


Figure 25. Position of the end nodes of the support tube under Z+ Curly folded and condition 1.

For the segmented inflatable model, the gas flowing into the CV3 and CV6 comes from CV2 and CV5, respectively. It can be seen from Figure 22 that the pressure in each cavity is the same during the deployment, which indicates that the inflatable gas flows fast. It can be seen from Figure 23 that the volume curves of CV1 and CV4 during the deployment were roughly the same, which was consistent with objective reality. The time history of the other four control volumes was also roughly the same. In the end, the volume of CV1 and CV4 was about twice of the others, which was in line with the actual situation. The process was relatively stable and smooth. However, it can be seen from Figure 24 that there was a certain distortion in the support tubes, which was also a disadvantage caused by adopting the curly-folded model, but the deployed effect was better. It can be seen from Figure 25 that the length of the support tubes adopting the Z-folded was longer than the Z-folded. Therefore, the Z-folded is a better choice for the solar sail at present.

In condition 2, the dynamic results of inflatable deployment are as follows in Figures 26–29:

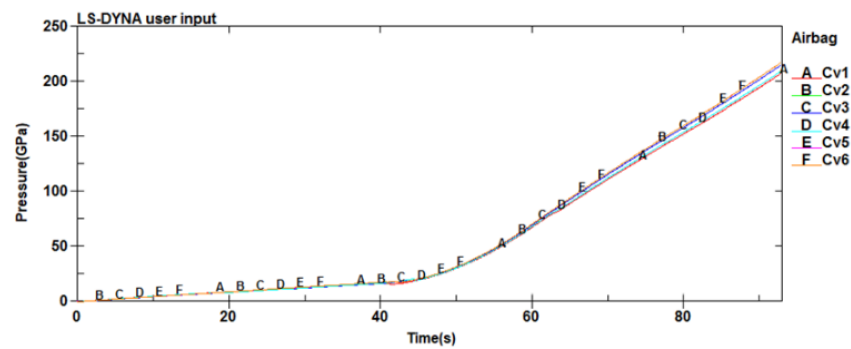


Figure 26. Pressure function curve of each tube under Z+ Curly folded and condition 2.

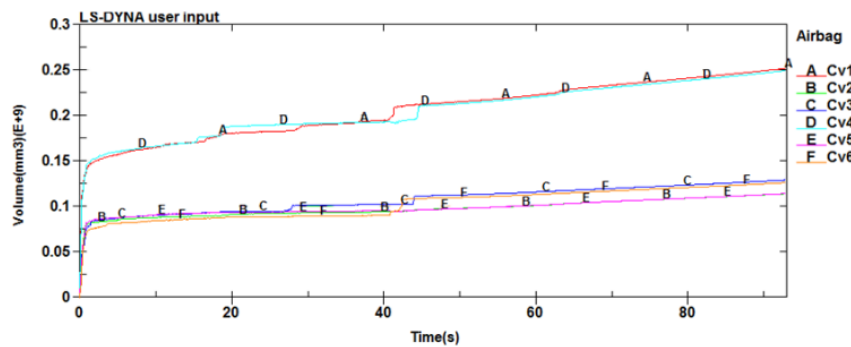


Figure 27. Volume function curve of each tube under Z+ Curly folded and condition 2.

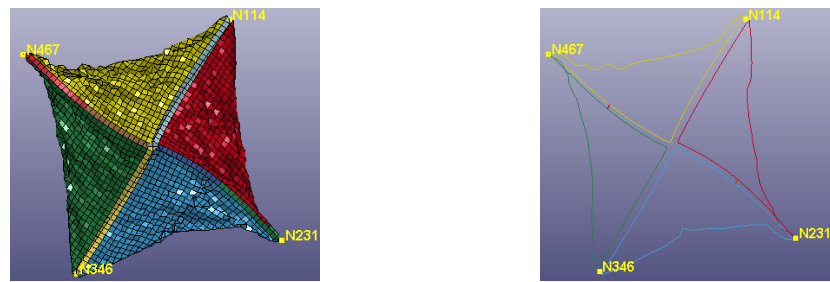


Figure 28. View of fully deployed under Z+ Curly folded and condition 2.

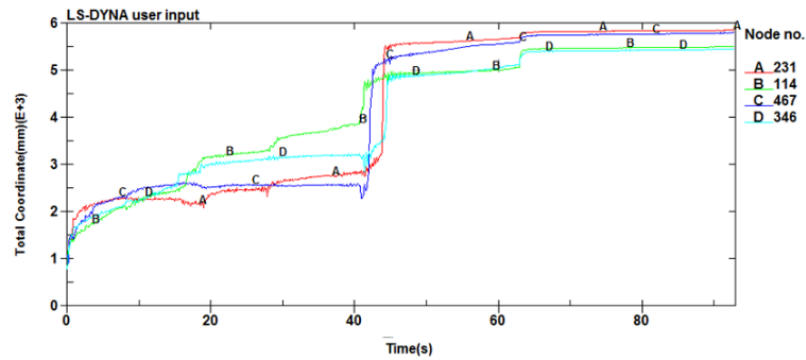


Figure 29. Position of the end nodes of the support tube under Z+ Curly folded and condition 2.

It can be seen from Figure 27 that the volume of each chamber increases slowly with time, showing a non-linear relationship. This is because when the inflation pressure exceeds the plastic stress of the diaphragm set at the connection of each chamber, the gas can flow to the next control volume, and the membrane structure can continue to unfold, which is consistent with the actual situation. In addition, it can be seen from Figure 26 that the pressure in each cavity was the same during the deployment. There was only a slight difference in the second half of the process, but it was not large. The process was relatively smooth. It was difficult to drive the sail surface to fully deploy by adopting the Z-folded due to the elastic modulus of the membrane structure is large. It can be seen from Figure 29 that the position of the end nodes of the support tubes that adopted the curly-folded method was smaller than that of the Z-folded, so it can be judged that the Z-folded is better.

In condition 3, the dynamic results of inflatable deployment are as follows in Figures 30–33:

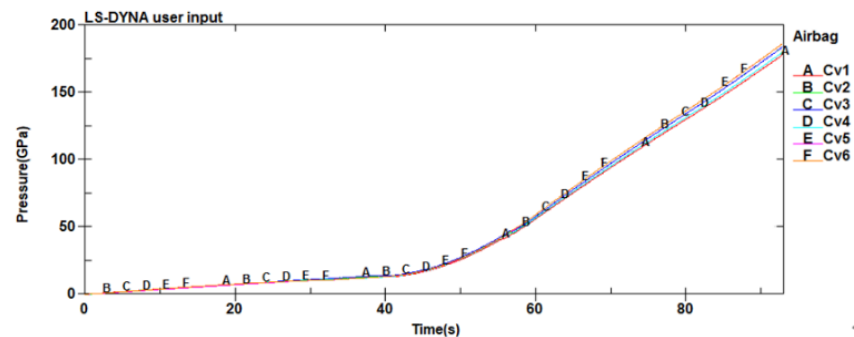


Figure 30. Pressure function curve of each tube under Z+ Curly folded and condition 3.

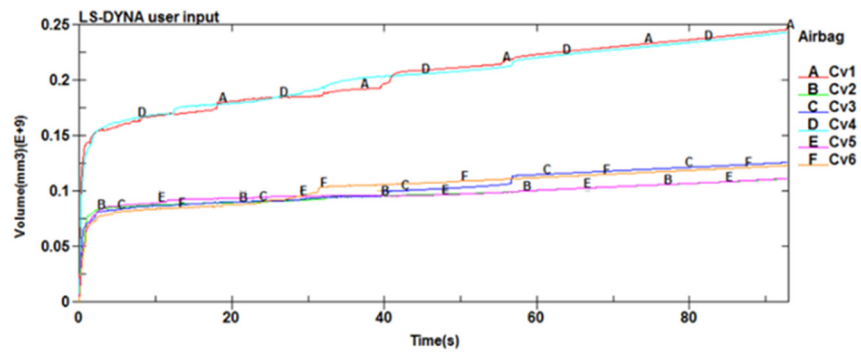


Figure 31. Volume function curve of each tube under Z+ Curly folded and condition 3.



Figure 32. View of fully deployed under Z+ Curly folded and condition 3.

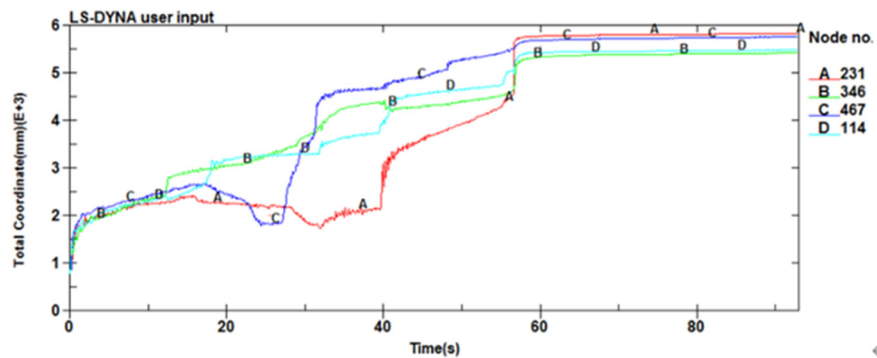


Figure 33. Position of the end nodes of the support tube under Z+ Curly folded and condition 3.

In this case, each control volume was inflated. Since the CV1 and CV4 were two times as large as the other control volumes, the load curves of CV1 and CV4 were twice larger than the remaining volumes.

In Figure 30, because the inflatable rate curve was proportional to cavity volume, the pressure was the same in each cavity. It can be seen from Figure 31 that the CV1 and CV4 were twice larger than the other cavities, which was consistent with the actual situation. The reason for this is that the gas load curve filled into each chamber is set in direct proportion to its volume. It can be seen from Figures 32 and 33 that the deployment was completed basically. However, the bending still existed in the support tubes which adopted curly folding, and this phenomenon was difficult to avoid.

In condition 4, the dynamic results of inflatable deployment are as follows in Figures 34–37:

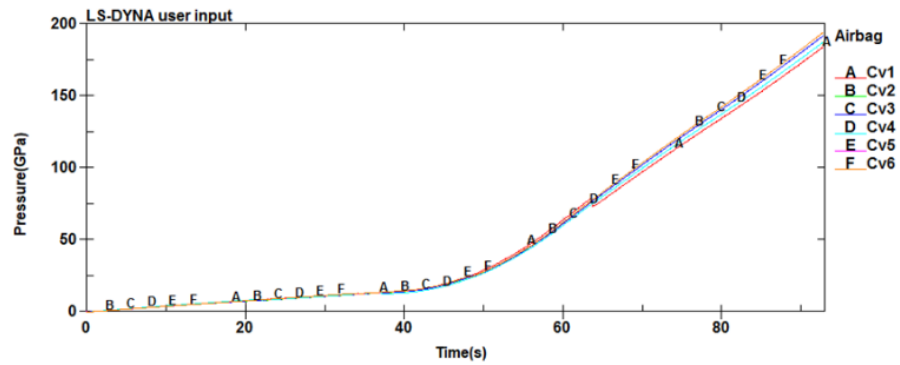


Figure 34. Pressure function curve of each tube under Z+ Curly folded and condition 4.

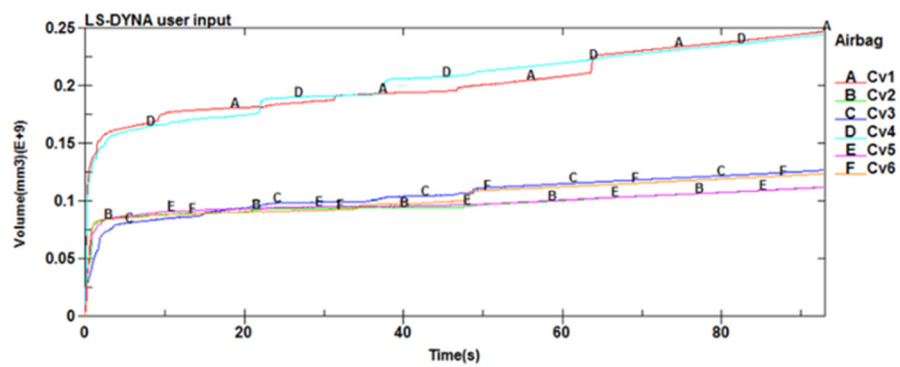


Figure 35. Volume function curve of each tube under Z+ Curly folded and condition 4.

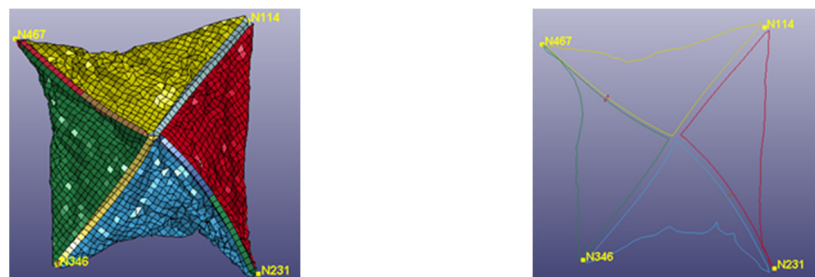


Figure 36. View of fully deployed under Z+ Curly folded and condition 4.

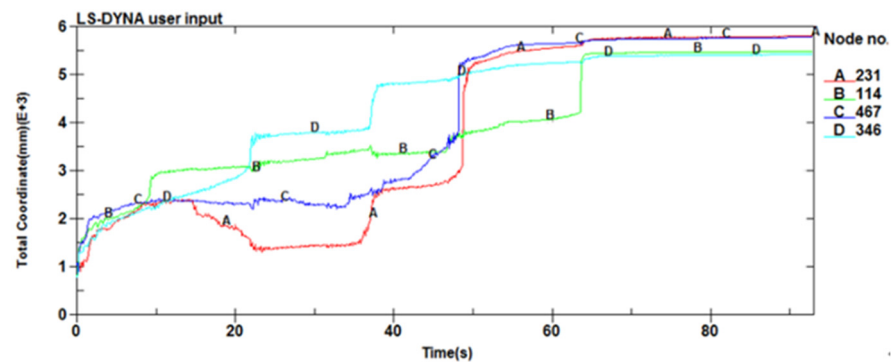


Figure 37. Position of the end nodes of the support tube under Z+ Curly folded and condition 4.

In summary, the solar sail was deployed, but it can be seen that the deployed effect of the support tubes where node 231 and node 467 were located was not ideal, especially since the one near node 231 had a large bend. As can be seen from Figure 37, the AC tubes were squeezed by the BD tubes during the initial inflation making the nodes displacement

of AC tubes tended to move back at about 30 s which caused the support tubes to slightly deform. Thus, the coefficient of friction can be set smaller in the contact keyword to prevent that situation.

In condition 5, the dynamic results of inflatable deployment are as follows in Figures 38–41:

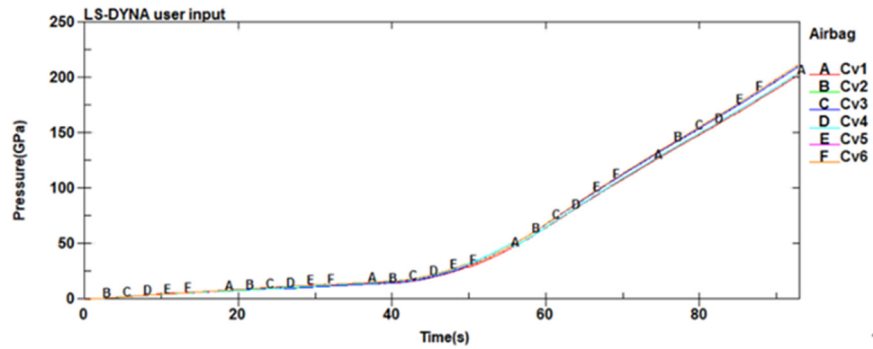


Figure 38. Pressure function curve of each tube under Z+ Curly folded and condition 5.

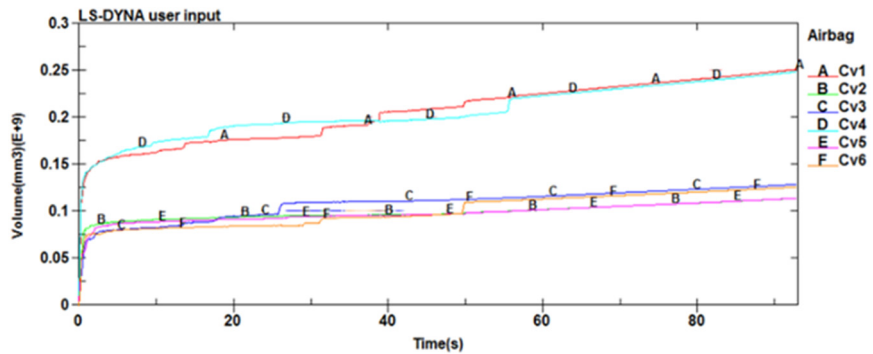


Figure 39. Volume function curve of each tube under Z+ Curly folded and condition 5.

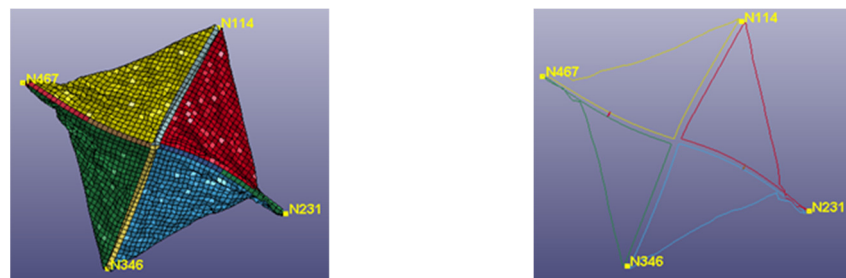


Figure 40. View of fully deployed under Z+ Curly folded and condition 5.

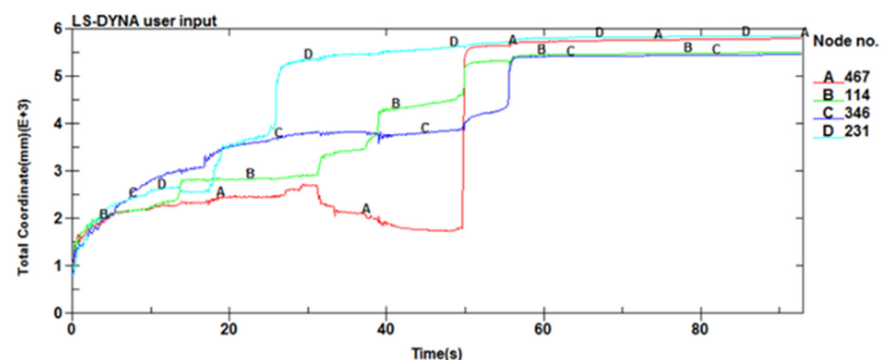


Figure 41. Position of the end nodes of the support tube under Z+ Curly folded and condition 5.

It can be seen from Figure 40 that the overall effect of the solar sail was better, but the sail surface near node 467 and node 231 did not deploy ideally. As it can be seen from Figure 41, there were still deformities on the structure under this condition, so the Z-folded model is not a good solution to deploy the solar sail.

#### 4. Conclusions

In this paper, the folded method of the solar sail was taken as the object. Based on the overall design of the structure, combining non-linear theory and finite element principles, two kinds of folded models of the solar sail were established in MSC.Patran, namely the Z-folded model and the Z+ curly-folded model. The dynamics deployed characteristics of the models were simulated and analyzed by LS-PREPOST, and the results were given under different conditions. The results showed by comparing and analyzing the pressure function curves, volume function curves, view of fully deployed, and the position of the end nodes during the deployment, that the Z-folded model is significantly better than the Z+curly-folded model. The model which adopted the Z+curly-folded had a certain distortion during the deployment, which makes the structure difficult to fully deploy, so it is not a good solution to apply. The model which adopted the Z-folded makes the structure deploy more straightly, the deployed flatness is better, and it is more suitable for practical applications.

**Author Contributions:** Conceptualization, L.Y.; methodology, L.Y. and R.S.; software, R.S. and F.W.; formal analysis, L.Y. and R.S.; data curation, R.S.; writing—original draft preparation, L.Y., R.S. and J.W.; project, J.L. All authors have read and agreed to the published version of the manuscript.

**Funding:** This research was funded by the National Science Fund for Distinguished Young Scholars (No. 11302134).

**Conflicts of Interest:** The authors declare no conflict of interest.

#### References

1. Glaser, R.; Gaccese, V.; Shahinpoor, M. Comparative finite element and experimental analysis of a quasi-static inflation of a thin deployable membrane space structure. *Finite Elem. Anal. Des.* **2018**, *138*, 48–65. [\[CrossRef\]](#)
2. Wei, J.; Ma, R.; Liu, Y. Modal analysis and identification of deployable membrane structures. *Acta Astronaut.* **2018**, *152*, 811–822. [\[CrossRef\]](#)
3. Wei, J.; Tan, H.; Wang, W. Deployable dynamic analysis and on-orbit experiment for inflatable gravity-gradient boom. *Adv. Space Res.* **2015**, *55*, 639–646. [\[CrossRef\]](#)
4. Yang, H.; Zhang, R.; Fan, Z.; Wang, Y.; Liu, R. Deploying dynamics experiment of tape-spring hinges for deployable mechanism. In Proceedings of the 2017 32nd Youth Academic Annual Conference of Chinese Association of Automation (YAC), Hefei, China, 19–21 May 2017; pp. 106–110.
5. Fernandez, J.M.; Lappas, V.J.; Daton-Lovett, A.J. Completely stripped solar sail concept using bi-stable reeled composite booms. *Acta Astronaut.* **2011**, *69*, 78–85. [\[CrossRef\]](#)
6. Brown, M.A. A deployable mast for solar sails in the range of 100–1000 m. *Adv. Space Res.* **2011**, *48*, 1747–1753. [\[CrossRef\]](#)
7. Qin, D. *Design and Analysis of Solar Sail Deployment Mechanism*; Springer: Shenyang, China, 2017.
8. Rong, S.; Liu, J.; Zhao, B.; Cui, N. Inflatable deployment dynamics simulation of Solar sail spacecraft support tube. In Proceedings of the 2009 International Conference on Mechatronics and Automation, Changchun, China, 9–12 August 2009; pp. 2239–2244.
9. Costanza, G.; Tata, M.E. Design and characterization of a small-scale solar sail deployed by NiTi Shape Memory actuators. *Procedia Struct. Integr.* **2016**, *2*, 1451–1456. [\[CrossRef\]](#)
10. Sprowitz, T.; Grundmann, J.T.; Seefeldt, P.; Spietz, P.; Hillebrandt, M.; Jahnke, R.; Mikulz, E.; Renger, T.; Reershemius, S.; Sasaki, K.; et al. Membrane Deployment Technology Development at DLR for Solar Sails and Large-Scale Photovoltaics. In Proceedings of the 2019 IEEE Aerospace Conference, Big Sky, MT, USA, 2–9 March 2019; pp. 1–20.
11. Roy, R.; Issac, K.K. Proposal for a light solar sail structure and its deployment. In Proceedings of the 2018 IEEE Aerospace Conference, Big Sky, MT, USA, 3–10 March 2018; pp. 1–16.
12. Johnson, L.; Whorton, M.; Heaton, A. NanoSail-D: A solar sail demonstration mission. *Acta Astronaut.* **2011**, *68*, 571–575. [\[CrossRef\]](#)
13. Fu, B.; Sperber, E.; Eke, F. Solar sail technology-A state of the art review. *Prog. Aerosp. Sci.* **2016**, *86*, 1–19. [\[CrossRef\]](#)
14. Sinn, T.; Vatile, M.; Tibert, G. Design and development of deployable self-inflating adaptive membrane. In Proceedings of the 53rd AIAA/ASME/ASCE/AHS/ASC Structures, Structural Dynamics, and Materials Conference, Honolulu, HI, USA, 23–26 April 2012; Volume 1517, pp. 23–26.

15. Fernandez, J.M.; Visagie, L.; Schenk, M. Design and development of a gossamer sail system for deorbiting in low earth orbit. *Acta Astronaut.* **2014**, *103*, 204–225. [[CrossRef](#)]
16. Sosa, E.M.; Wong, C.S.; Adumitroaie, A. Finite element simulation of deployment of large-scale confined inflatable structures. *Thin-Walled Struct.* **2016**, *104*, 152–167. [[CrossRef](#)]
17. Sosa, E.M.; Gregory, J. Experimental investigation of initial deployment of inflatable structures for sealing of rail tunnels. *Tunn. Undergr. Space Technol.* **2017**, *69*, 37–51. [[CrossRef](#)]
18. Pecora, L.; Sosa, E.M. FE simulation of ceiling deployment of a large-scale inflatable structure for tunnel sealing. *Thin-Walled Struct.* **2019**, *140*, 272–293. [[CrossRef](#)]
19. Lou, M.; Fang, H.; Hsia, L.M. A combined analytical and experimental study on space inflatable booms. In Proceedings of the 2000 IEEE Aerospace Conference. Proceedings (Cat. No.00TH8484), Big Sky, MT, USA, 25–25 March 2000; Volume 2, pp. 503–511.
20. Mallikarachi, H.M.Y.C.; Pellegrino, S. Deployment dynamics of ultrathin composite booms with tape-spring hinges. *J. Spacecr. Rocket.* **2014**, *51*, 604–613. [[CrossRef](#)]
21. Block, J.; Straubel, M.; Wiedemann, M. *Ultralight Deployable Booms for Solar Sails and Other Large GOSSAMER Structures in SPACE*; Elsevier Ltd.: Amsterdam, The Netherlands, 2011; Volume 68, pp. 984–992.
22. Li, Q.; Guo, X.; Gong, J. Experimental deployment behavior of air-inflated fabric arches and a full-scale fabric arch frame. *Thin-Walled Struct.* **2016**, *103*, 90–104. [[CrossRef](#)]
23. Ma, R.-Q.; Wei, J.-Z.; Tan, H.-F. Modal analysis of self-supporting arm with inflatable deployment. *J. Beijing Univ. Aeronaut. Astronaut.* **2018**, *44*, 526–534.
24. Zykov, A.V.; Legostayev, V.P.; Subbotin, A.V. The dynamics of a rotating solar sail when it is deployed. *J. Appl. Math. Mech.* **2015**, *79*, 35–43. [[CrossRef](#)]
25. Qian, P.; Chen, W.; Zhu, B.; Pan, J.; Hu, M. Research on Simulation Calculation of Kinematic Accuracy Reliability for Folding and Deploying Mechanism Considering Gaps of Kinematic Pair. In Proceedings of the 2012 Third International Conference on Digital Manufacturing & Automation, Guilin, China, 31 July–2 August 2012; pp. 703–706.
26. Zhang, X.; Zhou, C. Dynamic analysis of spinning solar sails at deployment process. *Chin. J. Aeronaut.* **2017**, *30*, 1719–1728. [[CrossRef](#)]
27. Rui, W.; Roberts, P.C.E.; Constantinos, S. Heliogyro solar sail with self-regulated centrifugal deployment enabled by an origami-inspired morphing reflector. *Acta Astronaut.* **2018**, *152*, 242–253.
28. Yang, C.; Zheng, W.; Zheng, X. Static and dynamic evaluations for large square solar sail concept based on scalable prototype validation. *Acta Astronaut.* **2019**, *159*, 258–266. [[CrossRef](#)]
29. Liu, J.; Cui, N.; Shen, F.; Rong, S.; Wen, X. Dynamic modeling and analysis of a flexible sailcraft. *Adv. Space Res.* **2015**, *56*, 693–713. [[CrossRef](#)]
30. Liu, J.; McInnes, C.R. Modulated solar pressure-based surface shape control of paraboloid space reflectors with an off-axis Sun-line. *Smart Mater. Struct.* **2018**, *27*, 035012. [[CrossRef](#)]